
LEVERAGING THREE-DIMENSIONALITY FOR NAVIGATION IN BLUFF-BODY WAKES

A PREPRINT

Vedasri Godavarthi^{1*}, Kartik Krishna², Steven L. Brunton², and Kunihiko Taira¹

¹Department of Mechanical and Aerospace Engineering, University of California, Los Angeles, CA 90095, USA

²Department of Mechanical Engineering, University of Washington, Seattle, WA 98195, USA

January 27, 2025

ABSTRACT

Biological flyers and swimmers navigate in unsteady wake flows using limited sensory abilities and actuation energies. Understanding how vortical structures can be leveraged for energy-efficient navigation in unsteady flows is beneficial in developing autonomous navigation for small-scale aerial and marine vehicles. Such vehicles are typically operated with constrained onboard actuation and sensing capabilities, making energy-efficient trajectory planning critically important. This study finds that trajectory planners can leverage three-dimensionality appearing in a complex unsteady wake for efficient navigation using limited flowfield information. This is revealed with comprehensive investigations by finite-horizon model-predictive control for trajectory planning of a swimmer behind a cylinder wake at $Re = 300$. The navigation performance of three-dimensional (3D) cases is compared to scenarios in a two-dimensional (2D) wake. The underactuated swimmer is able to reach the target by leveraging the background flow when the prediction horizon exceeds one-tenth of the wake-shedding period, demonstrating that navigation is feasible with limited information about the flowfield. Further, we identify that the swimmer can leverage the secondary transverse vortical structures to reach the target faster than is achievable navigating in a 2D wake.

1 Introduction

Small-scale aerial and marine vehicles are gaining traction in applications typically considered high-risk for manned vehicles. For these operations, vehicles need to traverse in unsteady flows, such as flying in urban environments [Watkins et al., 2020], in the wake of artificial and natural structures, navigating behind large marine vehicles for maritime operations [Shukla and Singh, 2019]. Such wake flows are associated with strong unsteady 3D vortical disturbances. Autonomous vehicles often experience adverse effects when encountering such flows without prior information [Zereik et al., 2018].

There have been studies on the effect of wake flows on the stability and performance of biological flyers and swimmers. The effect of 3D vortical perturbations generated by unsteady bluff body wakes on the aerodynamic coefficients and moments of insect flight and hummingbird flight show variable responses depending on the orientation and relative strength of the vortical perturbations [Ortega-Jimenez et al., 2014, Shyy et al., 2016]. The effect of three-dimensionality on locomotion is also studied in fish swimming [Liao, 2007, Lauder, 2015, Maia and Tytell, 2015] where fish undulate relative to the vortical structures for energy-efficient navigation. These studies have been conducted at high speeds and also consider the interaction between the swimmer/flyer with the flowfield. Understanding how the 3D flow structures can be leveraged for navigation offers insights into biological locomotion and the development of autonomous navigation strategies. Hence, we consider trajectory planning for laminar 3D wakes.

Over recent years, there has been extensive research on trajectory-planning strategies for the navigation of autonomous vehicles in complex background flows. Given complete knowledge of the underlying environment, optimization methods

*Corresponding author: vedasrig@g.ucla.edu

such as graph-based algorithms [Kularatne and Hsieh, 2016], and stochastic optimization [Lermusiaux, 2016] have been used to obtain optimal trajectories. Recently, reinforcement learning has been utilized for navigation in unsteady flows using limited local information [Colabrese et al., 2017, Gunnarson et al., 2021, Jiao et al., 2021]. Additionally, the Lagrangian coherent structures (LCS) theory has been used for energy-efficient path planning [Ross, 2008, Krishna and Brunton, 2022] proposed a finite-horizon model predictive control approach to identify energy-efficient trajectories and their connection to LCS for navigating unsteady flows.

In this study, we investigate the effect of three-dimensionality on navigation in unsteady wakes using the finite-horizon model predictive control approach used in Krishna and Brunton [2022]. We consider underactuated point swimmers to navigate in the 3D wake of a cylinder at a Reynolds number of 300, where the flow exhibits three-dimensionality due to secondary instabilities and compare their performance when navigating in 2D wakes. We reveal that secondary vortices in 3D flow facilitate faster navigation with limited information. The paper is outlined as follows. The computational setup and the flow physics of the cylinder flow are introduced in section 2. The finite-horizon model-predictive control approach is discussed in section 3. Section 4 provides the results for trajectory planning in cylinder wakes. The conclusions are given in section 5.

2 Computational setup

We consider a 3D incompressible wake behind a circular cylinder obtained from a direct numerical simulation (DNS) at a diameter (D) based on Reynolds number, $Re = U_\infty D / \nu$ of 300, where U_∞ and ν are freestream velocity and kinematic viscosity, respectively. The simulation is performed using the incompressible flow solver *Cliff*, (Cascade Technologies Inc.) based on a second-order accurate finite volume method for spatial discretization and a fractional-step method for time stepping [Iaccarino, 2004, Ham and Iaccarino, 2006]. The computational domain extends to $-20 \leq x/D \leq 30$ in the streamwise direction. The transverse extent is $-40 \leq y/D \leq 40$ and the spanwise extent is $0 \leq z/D \leq 4$ to capture the wavenumber of secondary instabilities with a uniform discretization of 80 grid cells and a timestep of $\Delta t = 0.005$. Hybrid grids are used with a structured mesh close to the cylinder and an unstructured mesh in the farfield region. We also obtain a 2D flow over a cylinder at the same Reynolds number using the same domain in the x , y directions. It amounts to about 0.1 and 8.3 million cells for both 2D and 3D wakes, respectively. Further details on the computational setup can be found in Kim et al. [2024]. For finite-horizon trajectory planning and visualization, we choose a subdomain $(x/D, y/D, z/D) \in [-2, 10] \times [-2, 2] \times [0, 2]$.

3 Finite-horizon model predictive control

We use a finite-horizon model predictive control (MPC) approach developed by Krishna and Brunton [2022] to perform trajectory optimization of a point swimmer. The swimmer dynamics is modeled as

$$\dot{\mathbf{x}}(t) = \mathbf{v}(\mathbf{x}(t), t) + \mathbf{u}(t), \quad (1)$$

where $\mathbf{x}, \mathbf{u} \in \mathbb{R}^n$ are the position vector and actuation velocity of the swimmer while \mathbf{v} is background flow velocity and $n = 2, 3$ for 2D and 3D flows. The background flow velocity is obtained from the DNS of the cylinder wake. When the actuation velocity is zero, the swimmer acts as a passive drifter. The swimmer dynamics is numerically integrated using a time step of $\Delta t = 0.05$. The actuation velocity is determined from the MPC optimization of the cost function given by

$$J = \int_{t_0}^{t_0+T_H} [\mathbf{e}(\tau)^T \mathbf{Q} \mathbf{e}(\tau) + \mathbf{u}(\tau)^T \mathbf{R} \mathbf{u}(\tau)] d\tau \quad (2)$$

subject to constraints on the component-wise actuation velocity with $|u_i(t)| \leq \eta_i$, where η_i is the actuation velocity bounds on i^{th} velocity component. Here, T_H is the time horizon over which the cost function is minimized, and \mathbf{e} is the error of the current state from a target state, $\mathbf{x}(t), \mathbf{e}(t) = \mathbf{x}(t) - \mathbf{x}_{\text{target}}$. The matrix $\mathbf{Q} \in \mathbb{R}^{n \times n}$ is positive semi-definite that penalizes the state error throughout the trajectory, and $\mathbf{R} \in \mathbb{R}^{n \times n}$ is a positive definite matrix penalizing the actuation effort. Here the actuation velocity of the swimmer is penalized, although the acceleration could also be optimized.

For the current problem, \mathbf{Q} is set to the identity matrix. When the actuation velocity is large i.e., $|\mathbf{u}| \geq U_\infty$ (freestream), the trajectory reaches the target directly. We consider underactuated scenarios to see how the swimmer exploits the background flow. The local background velocity for the cylinder wake varies in the streamwise, transverse, and spanwise (x, y, z) directions, with the streamwise velocity being dominant. Thus, the actuation efforts are penalized differently in different directions, and \mathbf{R} is a diagonal matrix where the i^{th} diagonal element is given as $R_{ii} = \gamma_i$ and γ_i is the actuation penalization in i^{th} direction. The time horizon T_H is another key parameter, as larger T_H requires larger predictive capabilities i.e., more temporal information about the background flow to the swimmer.

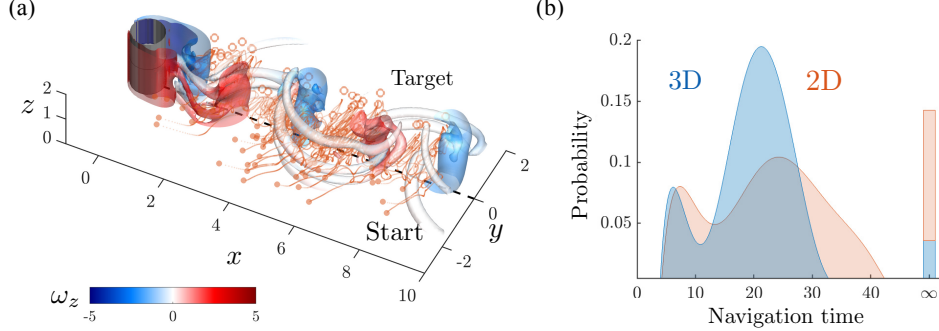


Figure 1: Trajectories of swimmers crossing the wake for 3D flow over a cylinder at $Re = 300$ visualized using iso-surface of Q -criterion $Q = 0.5$, colored by spanwise vorticity ω_z in (a) isometric view. (b) Probability distribution of total navigation time in 2D and 3D wakes.

4 Navigating three-dimensional wake flows

We consider trajectory planning for wake crossing in 2D and 3D cylinder wakes at $Re = 300$ as a canonical problem to examine the effect of three-dimensionality on swimmer navigation. At this Re , the secondary instabilities (referred to as modes A and B) result in three-dimensionality [Williamson, 1996]. Modes A and B are developed in the vortex cores (seen as less coherent spanwise vortices due to vortex tilting [Aleksyuk and Heil, 2023] and the braid regions between consecutive spanwise vortices (seen as streamwise-elongated vortices in figure 1(a)), respectively. These secondary instabilities result in the aperiodic nature of wake flow with a dominant frequency of $St = 0.202$, contrary to the periodic flow at a frequency $St = 0.212$ developed over a 2D cylinder at the same Re .

We consider wake-crossing scenarios (around 60 samples). These trajectories are shown in red in figure 1(a). The start (filled circles) and target transverse y locations are on either side of the cylinder wake ($y < 0$ for start and $y > 0$ for target positions) on the same spanwise plane. The streamwise x locations are chosen randomly in the cylinder wake. The background flow is initialized at the same phase of vortex shedding for both 2D and 3D flows. We consider five different initial phases of vortex shedding as the starting background flow for all the samples. Since the optimization function is performed for each component, the penalization for actuation velocity is also performed component-wise. For these wake-crossing scenarios, the swimmer is sensitive to actuation in a transverse direction, i.e., when not penalized in the transverse direction, the swimmer reaches the target in a straight line, as discussed later. Here, we present the underactuated cases with actuation bounds on the velocity as $0.9, 0.2, 0.5$ in the x, y, z directions with R_{ii} using $(\gamma_1, \gamma_2, \gamma_3) = (0.1, 10, 0.1)$. The time horizon for all cases is chosen as $T_H = 10\Delta t \approx 0.1T_p$, where T_p is the dominant wake-shedding period. The time horizon can also be measured relative to the size of the vortical structures in the flowfield. The wavelength of the mode B (Λ_B) instability, resulting in the braid-like region, is $\Lambda_B = 0.8D$ [Barkley and Henderson, 1996], hence this time horizon translates to 0.5 convective time units based on the diameter of the cylinder and 0.625 time units relative to the size of the braid-like structures. This indicates that flowfield information about one-half of the size of these vertical structures is enough for successful navigation. The obtained trajectories for $T_H \geq 0.1T_p$ indicate that the swimmers can reach the target when the time horizon is about at least one-tenth of a period. For $T_H = 10$, the same trends are observed for $0.85 \leq \eta_1 \leq 0.95, 0.1 \leq \eta_2 \leq 0.3, 0.1 \leq \eta_3 \leq 0.5$. An instance of the effect of spanwise actuation bounds on the swimmer trajectory is discussed in Appendix (depicted in figure 4). Since the optimization strategy minimizes $\|e(t)\|$ in equation (2), we consider the swimmer to be successful when $\|e(t)\| \leq \epsilon D$, which in this study is set to $\epsilon = 1/3$.

To compare the navigation performance in 2D and 3D wakes, we use the navigation time N_T , the time taken by the swimmer to reach the target, as a performance metric. The probability distribution of N_T for the sampled scenarios averaged over the three different initial background flow conditions is visualized in figure 1(b). We observe that distribution is shifted toward lower N_T for 3D wake navigation, identifying faster navigation in 3D wakes. The probability distribution also shows cases when $N_T \rightarrow \infty$ for unreachable scenarios. Thus the swimmers navigating in a 3D wake are more likely to reach the target position while being faster than those navigating in a 2D wake.

We divide the obtained trajectories into three scenarios as depicted in figure 2: (i) when the 3D navigation is faster than the 2D one (blue in figure 2(a)), (ii) when swimmers cannot reach the target (black in figure 2(b)) and (iii) when navigation in 2D is faster than in 3D wake (red in figure 2(c)). For (iii), the navigation time difference is approximately 20% of the wake shedding period ($-\Delta N_T < 0.2T_p$). The main difference between (i) and (iii) is the initial traverse locations y_0 (filled circles): for (i) they are outside of the wake whereas for (iii) the start locations are in the wake

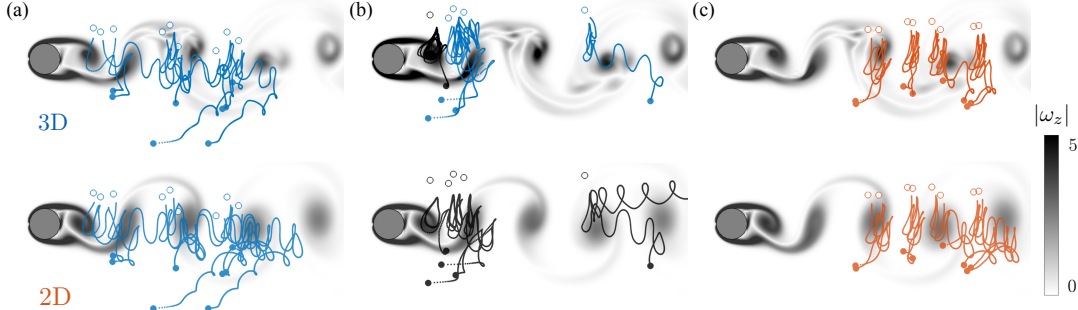


Figure 2: xy - view of wake crossing trajectories in 3D (top row) and 2D (bottom row) wakes visualized using $|\omega_z|$ for when (a) 3D navigation is faster (blue), (b) navigation in 2D cannot reach the target (black) and (c) navigation times in 2D and 3D wakes are similar (red).

region, resulting in lower background velocity from the start. From figures 2(a), the underactuated swimmer traverses significantly in the streamwise direction before reaching the target, whereas in figure 2(c) we observe that due to the current actuation parameters and the initial and target locations of the swimmer relative to the cylinder wake, the swimmer can directly cross the wake (almost in a straight line). This shows that streamwise navigation is faster in 3D wakes.

Figure 2(b) shows such cases where the swimmer fails to reach the target location in a 2D wake (black) but succeeds in a 3D wake (blue). The transverse target locations $y_{\text{target}} > 1.4D$ (unfilled circles) are farther from the wake, located in free-stream, for these cases. The 2D navigation with a finite horizon fails whereas the 3D wake navigation succeeds. Although the target locations are in free-stream, the secondary vortices in the braid regions in 3D wake provide low-velocity regions to reach the target, expanding the reachability boundaries. Even in a 3D wake, there are locations too far from the wake where the swimmer fails to reach the target for a given time horizon (shown by the leftmost trajectory in black in figure 2(b) (top)).

We now investigate the flow physics that the swimmer leverages for faster navigation in 3D wakes. We consider a scenario where 3D wake navigation is faster ($\Delta N_T > 0$) as depicted in figure 3(a)-(b) with an initial location of $x_0 = (4.34, -2.65, 1.0)$ (denoted by filled circle) and the target position of $x_{\text{target}} = (3.36, 0.29, 1.0)$ (denoted by unfilled circle) and $\Delta N_T = 8.3 \approx 1.8T_p$. In both 2D and 3D wake navigation, the swimmer initially travels downstream due to the lower actuation velocity of the swimmer compared to the background flow. A few time instants for the downstream navigation are shown in figure 3(c). We observe that the swimmer in a 3D wake "redirects" towards the goal earlier than that in a 2D wake as seen at $t = 17.5$, even though both the swimmers reach similar y locations. The swimmer in 2D wake travels farther downstream before it can redirect towards the target. Once the y location of the swimmer is in the cylinder wake, utilizing the low- background velocity the swimmer redirects and travels upstream in the wake towards the target as shown in figure 3(d). The swimmer trajectory oscillates in the x and y directions relative to the spanwise vortices in the cylinder wake, with fewer oscillations observed in 3D wake compared to 2D wake. The upstream navigation trajectory in the 2D wake in figure 3(b) is similar to the ones identified by Gunnarson et al. [2021], where the swimmer leverages the induced velocities in the x and y directions by the spanwise vortices.

The zoomed-in view of the time-instants when the swimmer in a 3D wake redirects towards the target (green box in figure 3(a)) and the time-instants of the swimmer navigating upstream (yellow box in figure 3(b)) are shown in figures 3(e)-(f). The instantaneous swimmer location (black dot) and its trajectory (grey) are shown relative to a transverse vortex (shown using ω_y) as it induces velocity in x and z directions. Figure 3(e) depicts the swimmer navigation under the influence of a counter-clockwise vortex. From, $t = 15.5$ to $t = 17$, the swimmer first travels in the negative z direction ($t = 16, 16.5$) and then travels in the upstream (negative x) direction, ($t = 17$) following the induced velocity and the background flow, thereby redirecting toward the upstream target earlier than its 2D counterpart.

For efficient upstream navigation in the 3D wakes, two mechanisms are in play: (i) the vorticity in the transverse and streamwise directions and (ii) the reduced coherence of spanwise vortices. Figure 3(f) depicts the swimmer navigation under the influence of a clockwise transverse vortex while traveling upstream in the wake. From $t = 23.25$ to $t = 24$, the swimmer first travels in the positive z direction and then in the negative x direction ($t = 23.5, 23.75$), leveraging the local orientation of background flow caused by the transverse vortex. This shows that the swimmer in a 3D wake travels in positive or negative z direction to effectively leverage the transverse vortices for upstream travel. The swimmer travels in the spanwise direction according to the orientation of subdominant transverse and streamwise vortices. These secondary vortices provide low-velocity regions and change the background flow orientation due to the induced velocity.

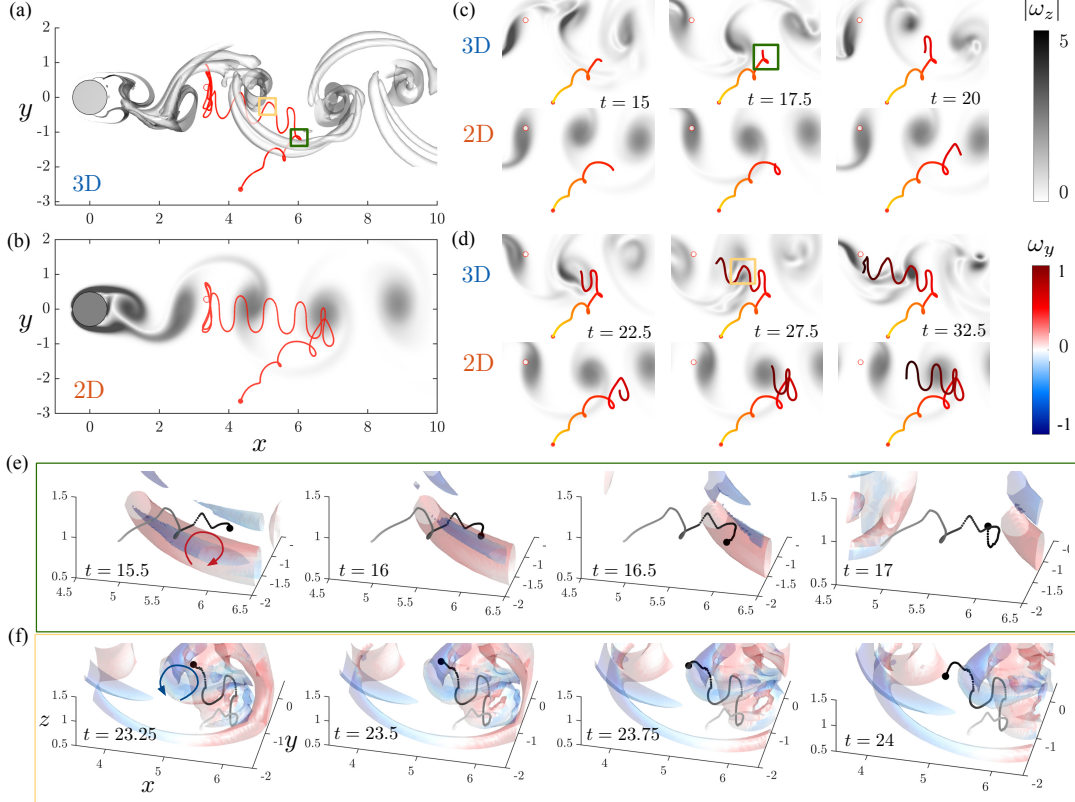


Figure 3: Trajectory optimization for a wake crossing scenario in (a) 3D and (b) 2D wake visualized using $|\omega_z|$. (c)-(d) Instantaneous trajectories during the navigation in 3D (top) and 2D (bottom) wakes. (e)-(f) Zoomed-in view of the evolution swimmer trajectory and background flow visualized using $Q = 0.1$ and colored using ω_y in 3D wake.

The swimmer leverages these vortices through the spanwise motion to effectively "redirect" toward the target for faster upstream navigation.

5 Conclusions

We investigated the influence of three-dimensionality on the navigation of underactuated swimmers in unsteady wakes using finite-horizon model predictive control for trajectory optimization. We compared the obtained trajectories for navigation in 2D and 3D cylinder wakes at $Re = 300$. For both scenarios, the time horizon needed to reach the target is only one-tenth of the wake-shedding period. This makes trajectory optimization for bluff-body wake navigation sensor-friendly. We also identified that the swimmer can navigate faster in 3D wakes compared with 2D wakes for most scenarios. Through spanwise motion, the swimmer can effectively leverage the secondary vortices, specifically transverse vortices to redirect towards the target faster. The low coherence of spanwise vortices and the presence of secondary vortices also facilitate faster upstream navigation when compared with 2D wake navigation.

Acknowledgments

We acknowledge funding from the US Air Force Office of Scientific Research (FA9550-21-1-0178). KT thanks the support from the US Department of Defense Vannevar Bush Faculty Fellowship (N00014-22-1-2798). We thank Youngjae Kim for providing the flowfield data and Kai Fukami for his valuable insights.

Declaration of interest

The authors report no conflict of interest.

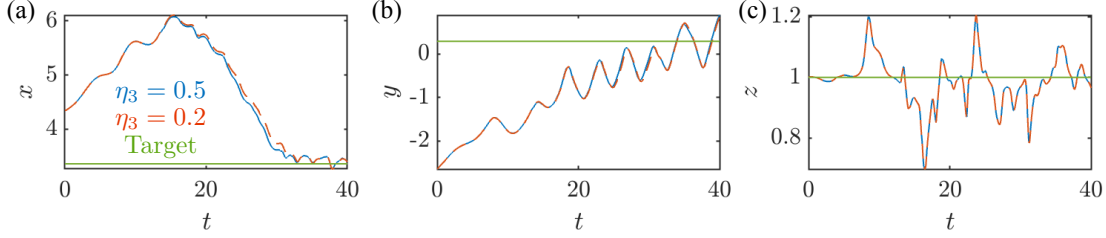


Figure 4: Trajectory evolution for a wake crossing scenario in 3D wake in the three-directions for different actuation bounds in z -direction (η_3).

Appendix

The underactuated swimmer trajectories shown in the main manuscript are obtained using the actuation bounds of $(\eta_1, \eta_2, \eta_3) = (0.9, 0.2, 0.5)$ in x , y and z directions respectively. While the lower actuation bound in the y direction is needed to avoid crossing the wake in a straight line, we here address the effect of actuation bounds in the spanwise direction. Let us consider the scenario discussed in figure 3. Figure 4 shows the trajectory evolution of the swimmer when $\eta_3 = 0.2$ (red) and $\eta_3 = 0.5$ (blue). Here, we use the same actuation bounds of $(\eta_1, \eta_2) = (0.9, 0.2)$ in x and y directions. We observe that both trajectories are similar irrespective of the difference in the actuation bound in the z direction. Since the secondary vortices are weaker than the spanwise vortices, the induced velocity by the secondary vortices in the z direction is also quite small, resulting in less actuation requirement in the z direction.

References

- S. Watkins, J. Burry, A. Mohamed, M. Marino, S. Prudden, A. Fisher, N. Kloet, and T. Jakobi & R. Clothier. Ten questions concerning the use of drones in urban environments. *Build. Environ.*, 167:106458, 2020.
- S. Shukla and S. S. Sinha & S. N. Singh. Ship-helo coupled airwake aerodynamics: a comprehensive review. *Prog. Aerosp. Sci.*, 106:71–107, 2019.
- E. Zereik, M. Bibuli, N. Mi sković, and P. Ridao & A. Pascoal. Challenges and future trends in marine robotics. *Annu. Rev. Control*, 46:350–368, 2018.
- V. M. Ortega-Jimenez, N. Sapir, M. Wolf, and E. A. Variano & R. Dudley. Into turbulent air: size-dependent effects of von kármán vortex streets on hummingbird flight kinematics and energetics. *Proc. Roy. Soc. B*, 281(1783):20140180, 2014.
- W. Shyy, C. K. Kang, P. Chirarattananon, and S. Ravi & H. Liu. Aerodynamics, sensing and control of insect-scale flapping-wing flight. *Proc. Roy. Soc. A*, 472(2186):20150712, 2016.
- J. C. Liao. A review of fish swimming mechanics and behaviour in altered flows. *Phil. Trans. Roy. Soc. B*, 362(1487):1973–1993, 2007.
- G. V. Lauder. Fish locomotion: recent advances and new directions. *Annu. Rev. of Mar. Sci.*, 7(1):521–545, 2015.
- A. Maia and A. P. Sheltzer & E. D. Tytell. Streamwise vortices destabilize swimming bluegill sunfish (*lepisomis macrochirus*). *J. Exp. Bio.*, 218(5):786–792, 2015.
- D. Kularatne and S. Bhattacharya & M. A. Hsieh. Time and energy optimal path planning in general flows. In *Robotics: Science and Systems*, pages 1–10. Ann Arbor, MI, 2016.
- D. N. Subramani & P. F. Lermusiaux. Energy-optimal path planning by stochastic dynamically orthogonal level-set optimization. *Ocean Model.*, 100:57–77, 2016.
- S. Colabrese, K. Gustavsson, A. Celani, and L. Biferale. Flow navigation by smart microswimmers via reinforcement learning. *Phys. Rev. Lett.*, 118(15):158004, 2017.
- P. Gunnarson, I. Mandralis, G. Novati, and P. Koumoutsakos & J. O. Dabiri. Learning efficient navigation in vortical flow fields. *Nat. Commu.*, 12(1):7143, 2021.
- Y. Jiao, F. Ling, S. Heydari, N. Heess, and J. Merel & E. Kanso. Learning to swim in potential flow. *Phys. Rev. Fluids*, 6(5):050505, 2021.
- C. Senatore & S. D. Ross. Fuel-efficient navigation in complex flows. In *American Control Conference*, pages 1244–1248. IEEE, 2008.

- K. Krishna and Z. Song & S. L. Brunton. Finite-horizon, energy-efficient trajectories in unsteady flows. *Proc. Roy. Soc. A*, 478(2258):20210255, 2022.
- F. Ham & G. Iaccarino. Energy conservation in collocated discretization schemes on unstructured meshes. *Annual Research Briefs*, 2004(3-14):118, 2004.
- F. Ham and K. Mattson & G. Iaccarino. Accurate and stable finite volume operators for unstructured flow solvers. *Annual Research Briefs*, 243, 2006.
- Y. Kim, V. Godavarthi, V. Rolandi, and J. Klamo & K. Taira. Influence of three-dimensionality on wake synchronisation of an oscillatory cylinder. *J. Fluid Mech.*, 1001:A24, 2024.
- C. H. K Williamson. Three-dimensional wake transition. *J. Fluid Mech.*, 328:345–407, 1996.
- A. I. Aleksyuk and M. Heil. On the onset of long-wavelength three-dimensional instability in the cylinder wake. *J. Fluid Mech.*, 967:A23, 2023.
- D. Barkley and R. D. Henderson. Three-dimensional floquet stability analysis of the wake of a circular cylinder. *J. Fluid Mech.*, 322:215–241, 1996.